CHAPTER

# 4 RESULTS & DISCUSSION

## 4.1 Introduction

The development and methodology of a novel front-end noise power and SNR estimation technique for AWGN channel in OFDM systems has been described in the last chapter. The technique is also extended to obtaining noise power estimates of colored noise using wavelet-packet based filter bank analysis of the noise. This technique is very useful in obtaining the best SNR estimates that are made use of in optimal deployment of OFDM. OFDM technology requires knowledge of the SNR for optimal performance. For instance, in OFDM systems, SNR estimation is used for power control, adaptive coding and modulation, turbo decoding etc.

In this chapter, we present results of the proposed front-end noise power and SNR estimation technique for white noise and for colored noise. In order to benchmark the proposed noise power and SNR estimation technique, a complete end-to-end fixed-broadband-wireless-access-system based on IEEE802.16d simulation has been developed in chapter 3. The simulations are conducted in both frequency non-dispersive and dispersive channels with real additive white Gaussian noise (AWGN) and also colored noise.

The results of SNR estimation technique for AWGN in OFDM systems are shown in section 4.2 and compared with other techniques in terms of normalized mean squared

error (NMSE) and estimated SNR. In section 4.3, the results of SNR estimation technique for colored noise using wavelet-packet in OFDM systems are shown and compared with previous techniques in terms of mean squared error (MSE) and estimated SNR.

## 4.2 Analysis Results of SNR Estimation Technique for Multipath Channels With AWGN in OFDM Systems

As depicted in chapter 3 on methodology, the proposed SNR estimation technique is hereby evaluated in terms of following criteria.

1. **Performance Evaluation:** This criterion is to establish how good an estimate the technique can provide. Towards this end, we provide comparison of estimated SNR with actual SNR and we also provide normalized mean squared error (NMSE) between actual SNR and estimated SNR at various SNR levels for our technique as well as other techniques. We extend this to predict the performance under various channel conditions. Furthermore, we extend the technique to perform even in colored noise, and evaluate its performance.

2. **Computational Complexity:** Towards this end, we compute the number of multiplications needed to get the SNR estimate and compare that with other techniques.

3. **Sensitivity Analysis:** Towards this end, we analyze which parameter our technique is more sensitive to.

### 4.2.1 Performance Evaluation

For fixed broadband wireless access systems characterized by IEEE802.16d, OFDM training / synchronization data of length $N=256$ is sent from the transmitter ($T_x$) where The cyclic prefix length is chosen as $l_{CP}$=64, so that $N_{total}$=320. The other parameters for the simulations are given in Table 3.3 of chapter 3. The proposed SNR estimator is

compared with two existing SNR estimators, the Reddy estimator [Reddy et al, 2003] and Subspace based estimator [Xiaodong et al, 2005] in terms of normalized mean squared error (NMSE) and estimated SNR. SNR is varied from 1 dB to 16 dB and the normalized mean-squared error (NMSE) is derived for the estimated SNR. In order to statistically accurate, mean is obtained over 2000 samples according to the following formula

$$NMSE = \frac{1}{2000} \sum_{m=1}^{2000} \left( \frac{\hat{SNR} - SNR}{SNR} \right)^2 \quad (4.1)$$

The NMSE results shows that proposed estimator with one OFDM symbol performs better than both Reddy's and subspace estimator which gives accurate SNR estimates after an observation interval of 20 OFDM symbols. The performance of proposed estimator (using one OFDM symbol) is compared with Reddy estimator (using 30 OFDM symbols) and subspace estimator (using 30 OFDM symbols). The performance is evaluated via computer simulations using AWGN channel. The results are shown in the Fig 4.1 and Fig 4.2 for SNR-NMSE vs. SNRdB and estimated SNR vs. actual SNRdB. Results shows that the proposed estimator provides enhanced performance in SNR estimation as compared to Reddy and subspace estimators.

The proposed estimator also performs well with other multipath channels (Rayleigh, rician, SUI channels, indoor channel models). The simulations are performed using this multipath channel with different number of taps and results are shown in Figs.4.3 to 4.30. Description of multipath taps used by our technique are given in Table 4.1. It is observed that the performance of proposed estimator is good in terms of NMSE and estimated values of SNR. The results of SUI channels and indoor channel models shows that the proposed technique also performs better estimation of SNR for Wi-Fi (IEEE802.11a) and WiMAX (IEEE802.16, 2004) systems.

In WiMAX (IEEE802.16, 2004) systems, the channel is modeled by the 6 SUI multipath channels with additive white Gaussian noise (AWGN) added to the time samples [Erceg

et al, 2003]. The 6 channels model the typical channels for 3 types of terrains. Terrain type A is hilly terrain with moderate-to-heavy tree densities while type C is flat terrain with light tree densities. Terrain type B is intermediate between type A and terrain type C. Table4.2 shows the terrain type and corresponding SUI channels that represent them. Table 4.3 shows the description of SUI channels used in our simulations.

It is also seen that the performance of proposed estimator is good with Wi-Fi systems (IEEE802.11a) with indoor channel models of 10 taps. Values of taps are taken from the indoor channel models developed by Zhao [Zhao, 2004]. Description of these channel models are given in Table 4.4.

**Table 4.1: Description of Rayleigh and Rician channel**

| | **Taps for Rayleigh Channel & Rician Channel** | | | | | | | | | | **Unit** |
|---|---|---|---|---|---|---|---|---|---|---|---|
| **3-Taps** | **Delay** | 0 | | 1.5 | | 3.2 | | | | | µ sec |
| | **Power** | 0 | | -15 | | -30 | | | | | dB |
| | **K-Factor** | 10 ( K=0 for Raleigh channel) | | | | | | | | | |
| **5-Taps** | **Delay** | 0 | | 1.5 | | 3.2 | | 4.5 | | 6 | µ sec |
| | **Power** | 0 | | -15 | | -25 | | -35 | | -45 | dB |
| | **K-Factor** | 10 ( K=0 for Raleigh channel) | | | | | | | | | |
| **10-Taps** | **Delay** | 0 | 1.5 | 3.2 | 4.5 | 6 | 7.5 | 10 | 13 | 16 | 19 | µ sec |
| | **Power** | 0 | -5 | -10 | -15 | -20 | -30 | -45 | -60 | -70 | -80 | dB |
| | **K-Factor** | 5 ( K=0 for Raleigh channel) | | | | | | | | | | |

**Table 4.2: Terrain types and corresponding SUI channels**

| **Terrain Type** | **SUI-Channels** |
|---|---|
| *C* | *SUI-1, SUI-2* |
| *B* | *SUI-3, SUI-4* |
| *A* | *SUI-5, SUI-6* |

**Table 4.3: Description of SUI channels**

| | | Tap1 | Tap2 | Tap3 | Unit |
|---|---|---|---|---|---|
| **SUI-1** | **Delay** | 0 | 0.4 | 0.9 | µ sec |
| | **Power** | 0 | -21 | -32 | dB |
| | **K-Factor** | 16 | | | |
| **SUI-2** | **Delay** | 0 | 0.4 | 1.1 | µ sec |
| | **Power** | 0 | -18 | -27 | dB |
| | **K-Factor** | 8 | | | |
| **SUI-3** | **Delay** | 0 | 0.4 | 0.9 | µ sec |
| | **Power** | 0 | -11 | -22 | dB |
| | **K-Factor** | 3 | | | |
| **SUI-4** | **Delay** | 0 | 1.5 | 4 | µ sec |
| | **Power** | 0 | -10 | -20 | dB |
| | **K-Factor** | 1 | | | |
| **SUI-5** | **Delay** | 0 | 4 | 10 | µ sec |
| | **Power** | 0 | -11 | -22 | dB |
| | **K-Factor** | 2 | | | |
| **SUI-6** | **Delay** | 0 | 14 | 20 | µ sec |
| | **Power** | 0 | -16 | 26 | dB |
| | **K-Factor** | 2 | | | |

**Table 4.4: Description of Indoor channel models for Wi-Fi**

| **10 Taps for Indoor Channel Models** | | | | | | | | | | | **Unit** |
|---|---|---|---|---|---|---|---|---|---|---|---|
| **Delay** | 0 | 10 | 20 | 30 | 40 | 50 | 70 | 90 | 110 | 130 | n-sec |
| **power** | 0 | -1.8 | -3.8 | -4.4 | -5 | -6 | -10 | -11.8 | -13 | -15 | dB |
| **K-Factor** | 10 | | | | | | | | | | |

### 4.2.1.1 Comparison with Other Techniques

In Fig. 4.1 is shown the normalized mean squared error between estimated SNR and actual SNR (SNR-NMSE) plotted against actual SNR. These results are compared with those of Reddy and subspace.

It can be seen from the Fig.4.1, that the proposed technique has very small NMSE error as compared to Reddy and Subspace. The proposed estimator makes use of only one OFDM symbol unlike Reddy and subspace method which are using 30 OFDM symbols. It is observed that the rise in NMSE at small SNR is due to window effect of the system.

In Fig 4.2 estimated SNR is plotted against actual SNR and compared with Reddy's and subspace techniques**.**

It is clear from the plot that the proposed estimator gives SNR estimates that have very small bias and are very close to actual SNR value. It is observed that Reddy's technique and subspace technique have more bias in their estimates as compared to our proposed technique.

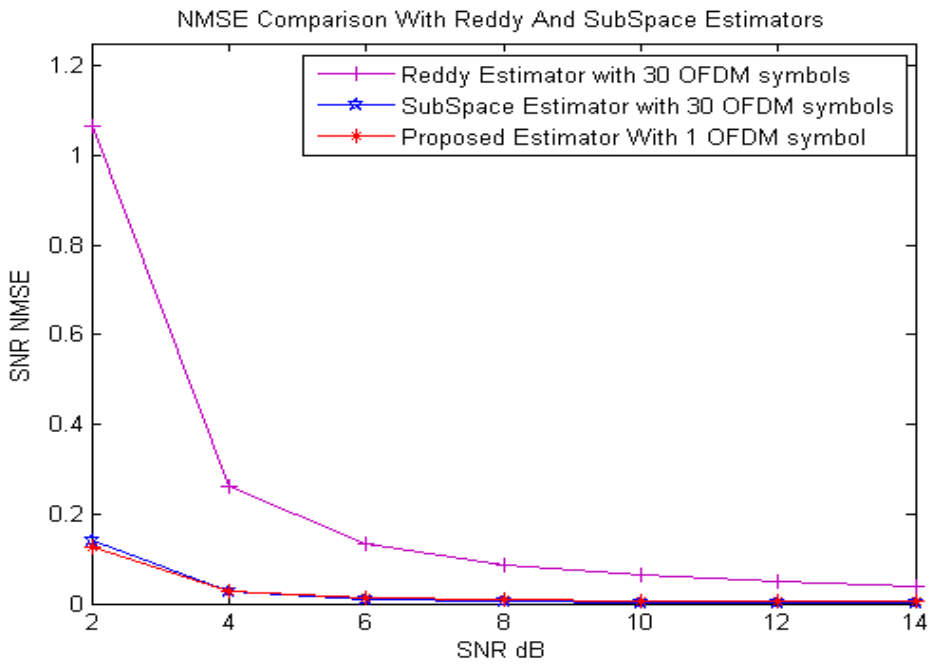


**Fig.4.1 SNR-NMSE vs. actual SNR comparison of proposed technique with Reddy's and subspace Estimators**

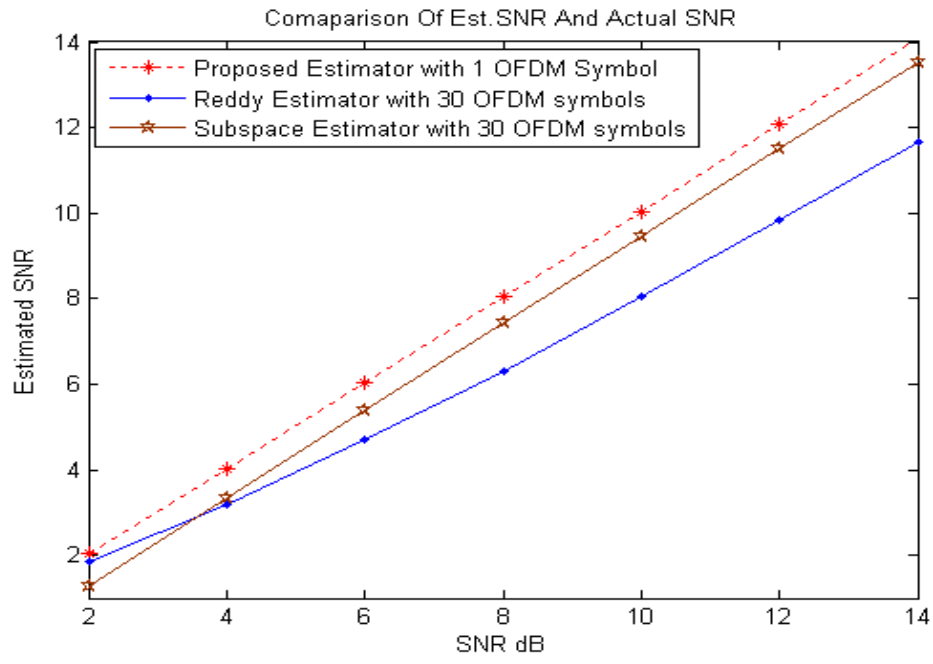


**Fig.4.2 Estimated SNR vs. actual SNR comparison of proposed technique with Reddy's and subspace**

### 4.2.1.2 Performance over AWGN, Rayleigh and Rician

In Fig. 4.4 is shown the SNR-NMSE is plotted against actual SNR using AWGN channel.

It can be seen from the Fig.4.4, that the proposed technique has very small NMSE error. It is observed that the rise in NMSE at small SNR is due to window effect of the system.

In Fig. 4.5 estimated SNR is plotted against actual SNR for AWGN channel. It can be seen that the SNR estimates are very less bias and are very close to the actual SNR.

Fig. 4.6 to Fig. 4.17 performance over Rayleigh and Rician channel for 3 taps, 5 taps and 10 taps, is shown in terms of SNR-NMSE and estimated SNR. The description of Rayleigh and Rician channels is shown in Table 4.1.

It can be seen from the figures, that the proposed technique perform well with Rayleigh and Rician multipath channels and has very small NMSE error. The NMSE is consistently seen to be more for low SNRs. The error could be due to the finite size of the data-window or equivalently, bandwidth window. The effect of finite width window is seen in Fig. 4.3 where autocorrelation of AWGN over the same bandwidth is plotted. As can be seen from figure, the autocorrelation is not zero at delays $\tau \neq 0$. These non zeros values can corrupt the measurement of peaks and cause error.

It also can be seen from these figures that the SNR estimates have very small bias and are very close to the actual SNR.

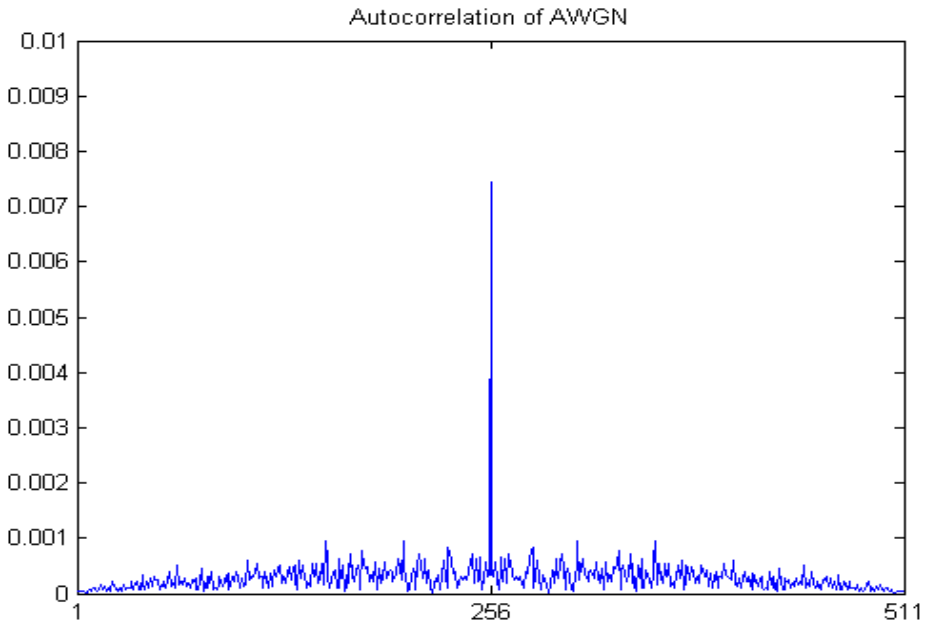


**Fig. 4.3 Autocorrelation of AWGN**

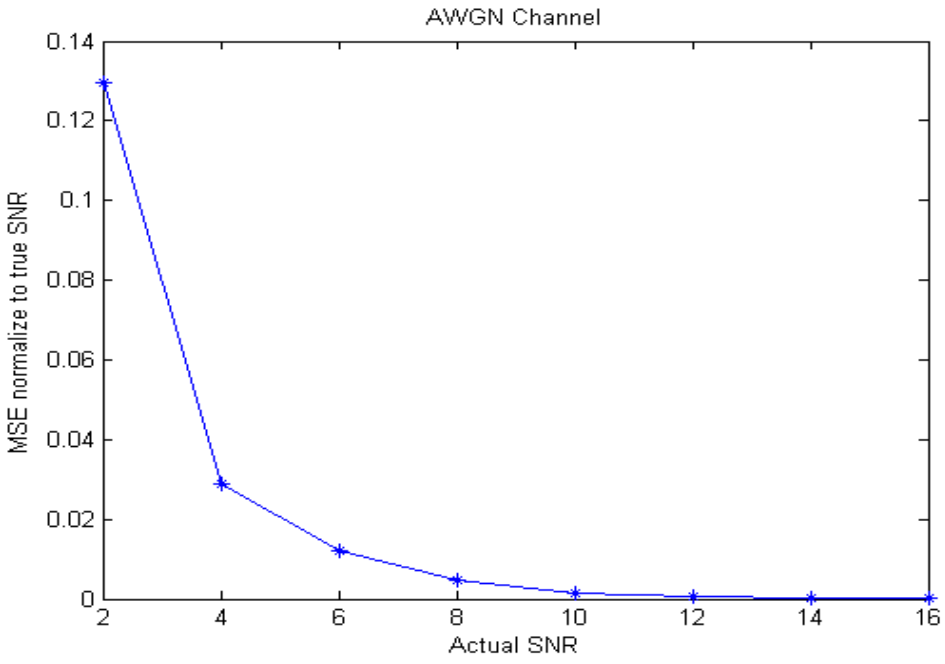


**Fig.4.4 SNR-NMSE vs. actual SNR with AWGN channel**

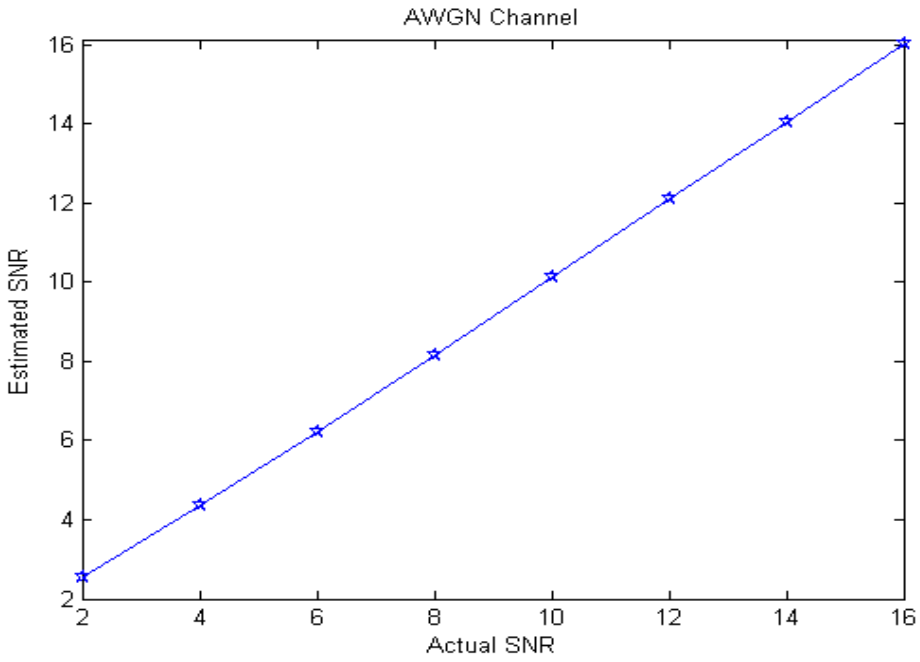


**Fig.4.5 Estimated SNR vs. Actual SNR with AWGN channel**

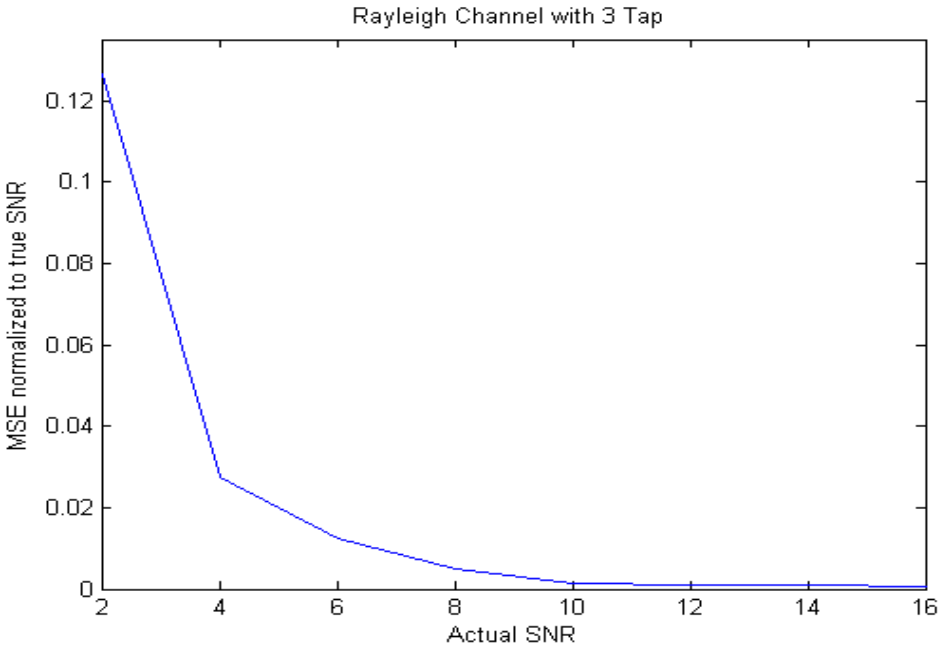


**Fig.4.6SNR-NMSE vs. actual SNR with Rayleigh 3-Tap channel**

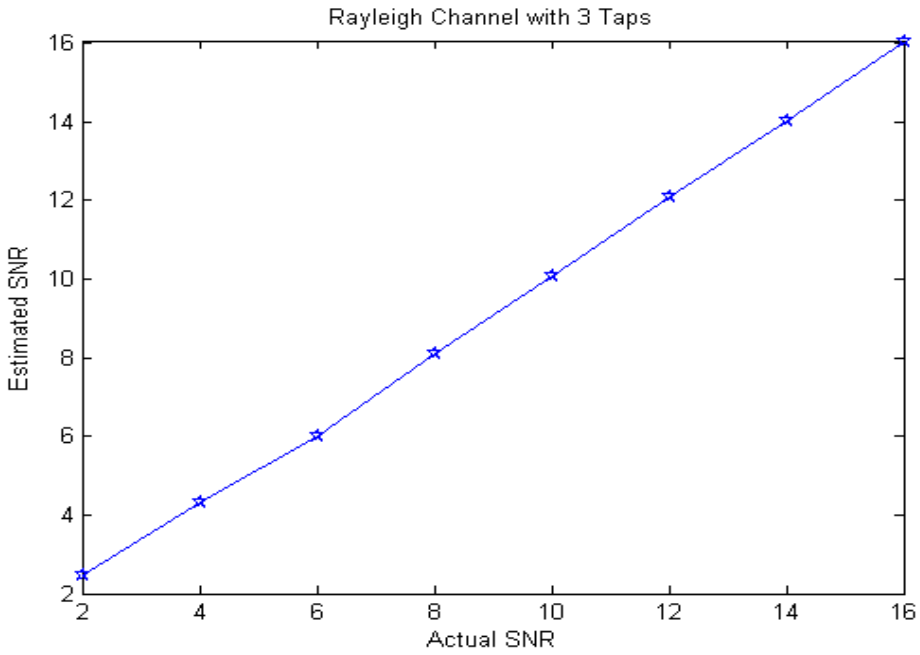


**Fig.4.7 Estimated SNR vs. Actual SNR with Rayleigh 3-Tap channel**

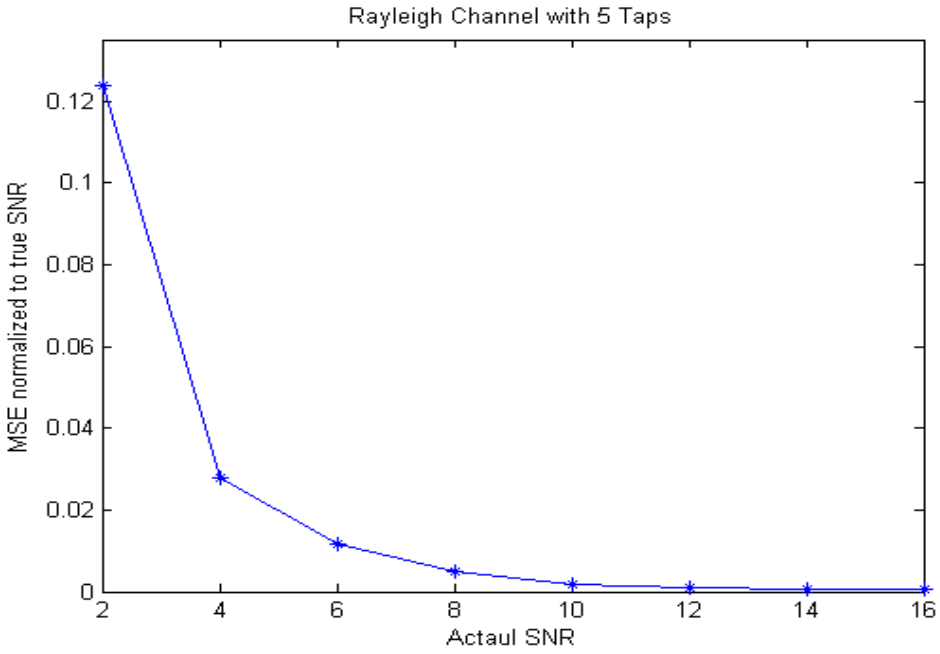


**Fig.4.8 SNR-NMSE vs, actual SNR with Rayleigh 5-Tap channel**

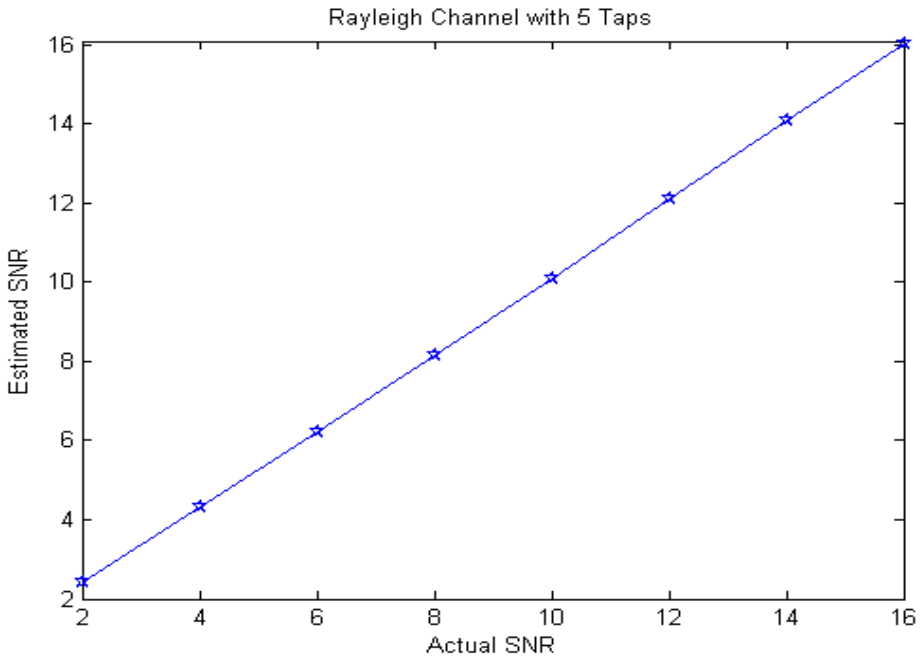


**Fig.4.9 Estimated SNR vs. Actual SNR with Rayleigh 5-Tap channel**

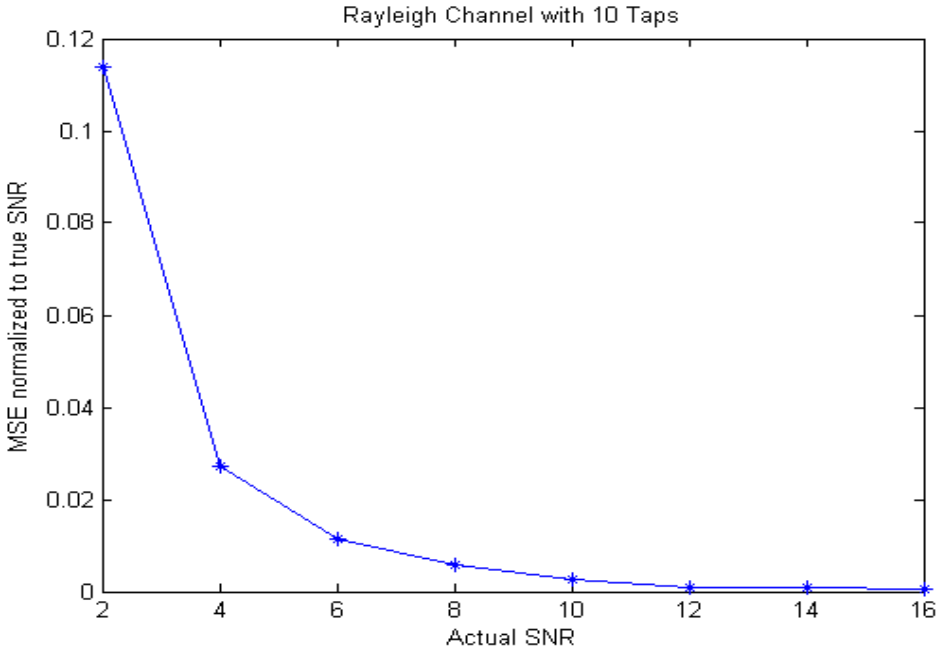


**Fig.4.10 SNR-NMSE vs. actual SNR with Rayleigh 10-Tap channel**

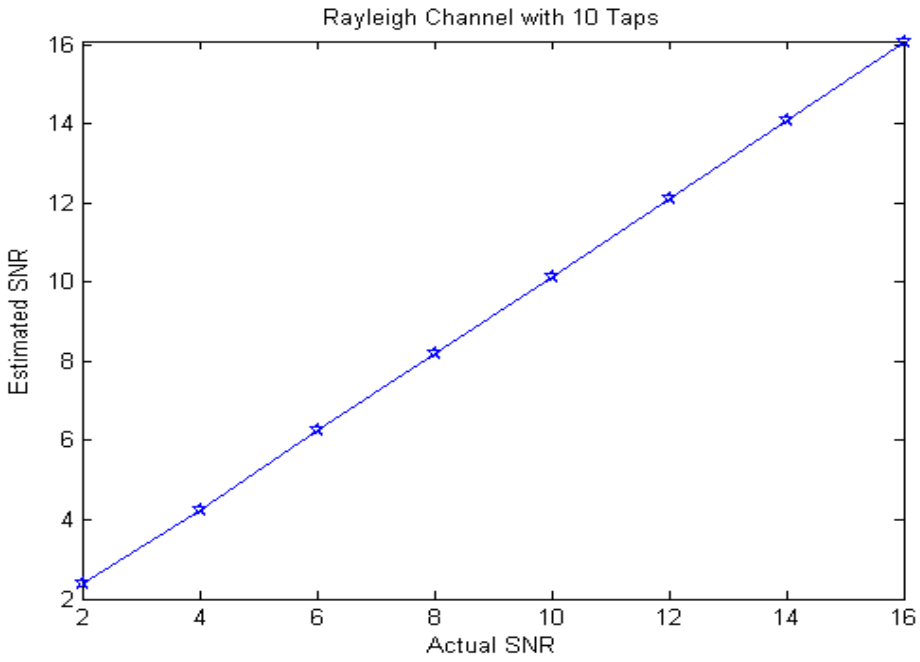


**Fig.4.11 Estimated SNR vs. Actual SNR with Rayleigh 10-Tap channel**

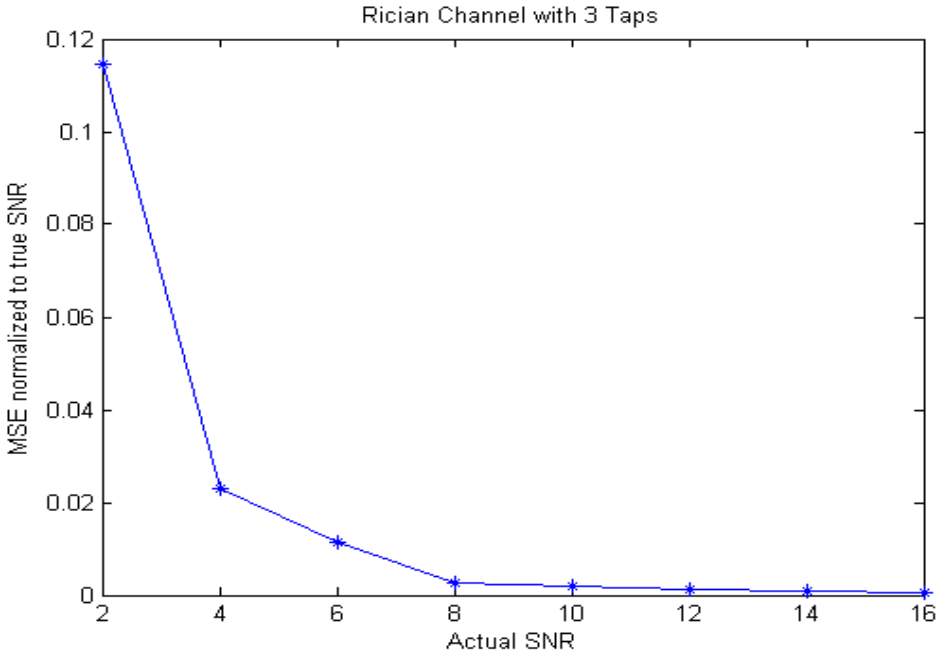


**Fig.4.12 SNR-NMSE vs. actual SNR with Rician 3-Tap channel**

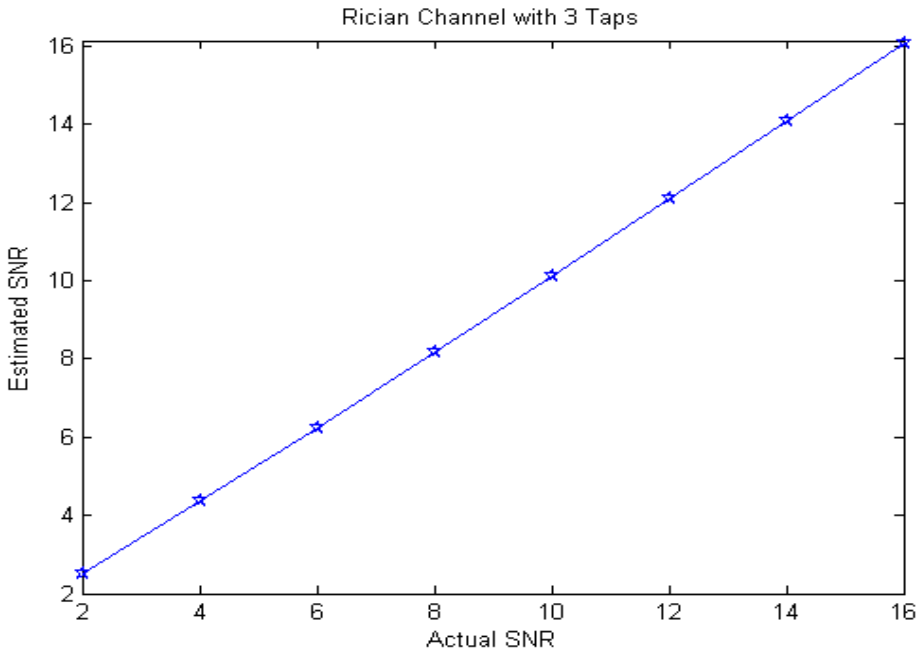


**Fig.4.13 Estimated SNR vs. Actual SNR with Rician 3-Tap channel**

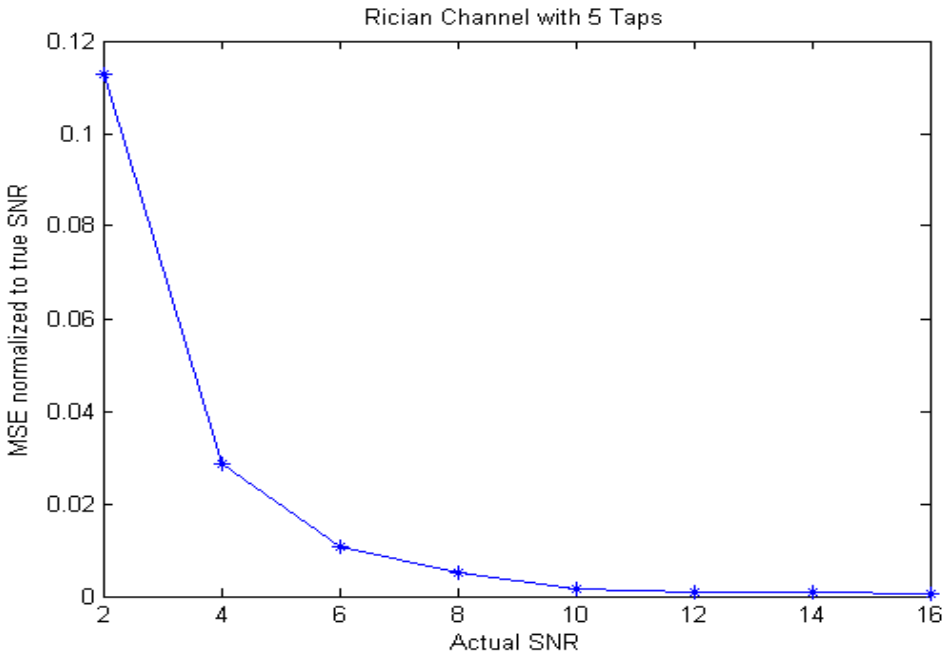


**Fig.4.14 SNR-NMSE vs. actual SNR with Rician 5-Tap channel**

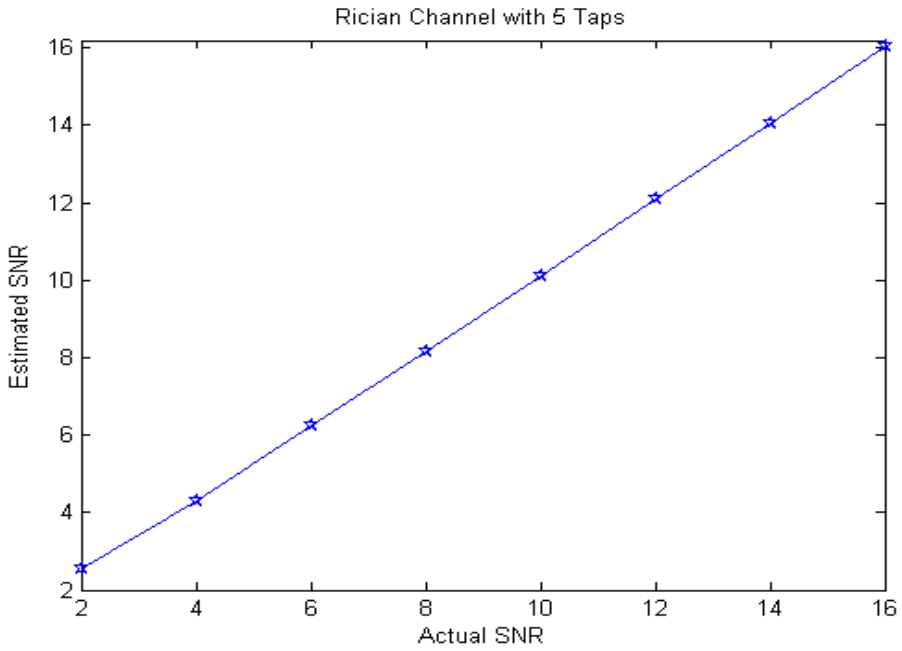


**Fig.4.15 Estimated SNR vs. Actual SNR with Rician 5-Tap channel**

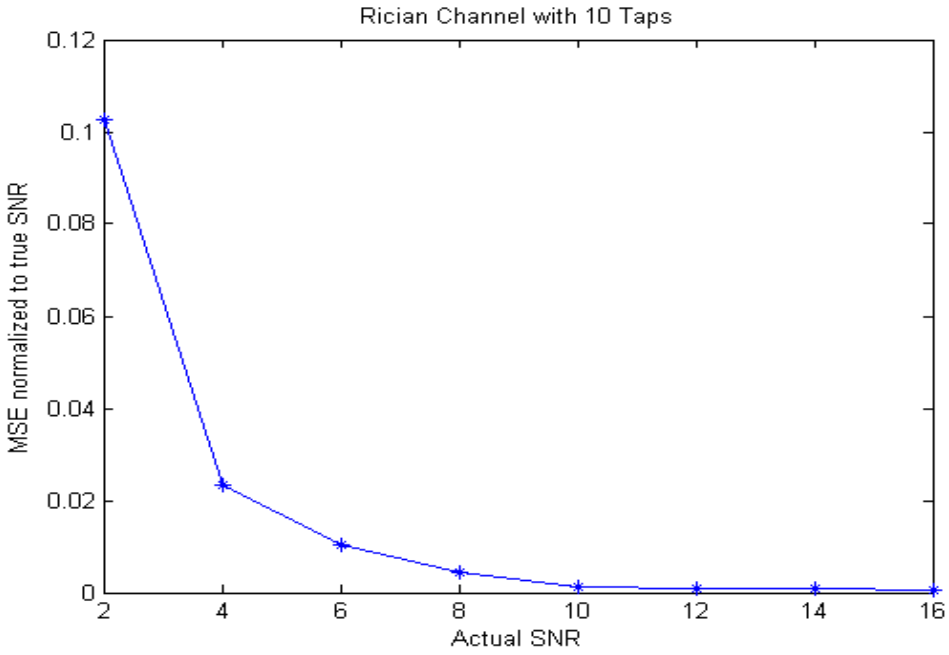


**Fig.4.16 SNR-NMSE vs. actual SNR with Rician 10-Tap channel**

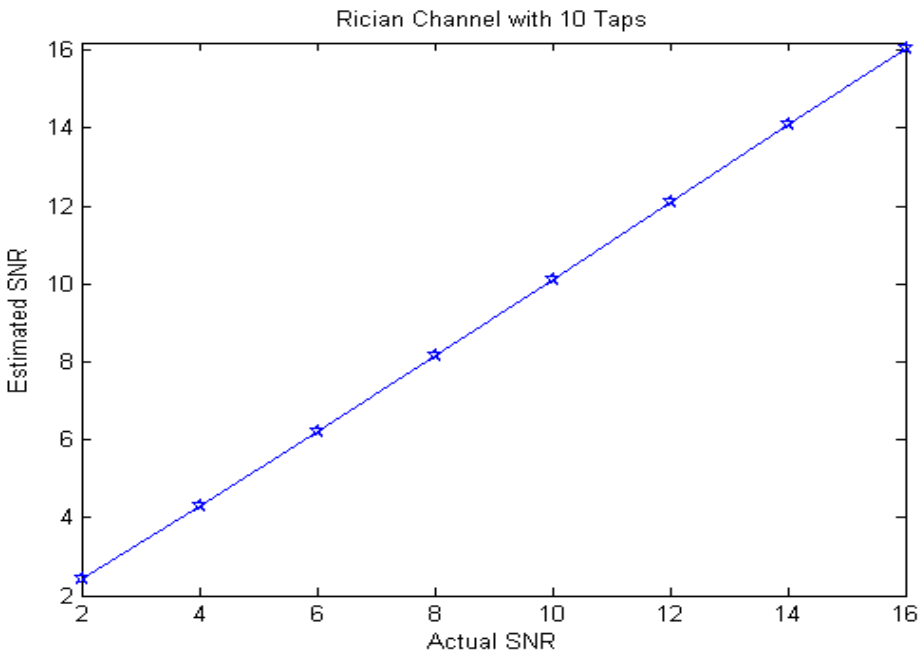


**Fig.4.17 Estimated SNR vs. Actual SNR with Rician 10-Tap channel**

### 4.2.1.3 Performance over SUI Multipath Channels

Fig 4.18 to Fig 4.29 performance over SUI multipath channel for 3 taps is shown in terms of SNR-NMSE and estimated SNR. The description of SUI multipath channels is shown in Table 4.3.

It can be seen from the Fig 4.18 to Fig 4.29, that the proposed technique perform well with SUI multipath channels and have very small NMSE error. It is observed that the rise in NMSE at small SNR is due to window effect of the system.

It also can be seen from these figures that the SNR estimates have very small bias and have very close to the actual SNR.

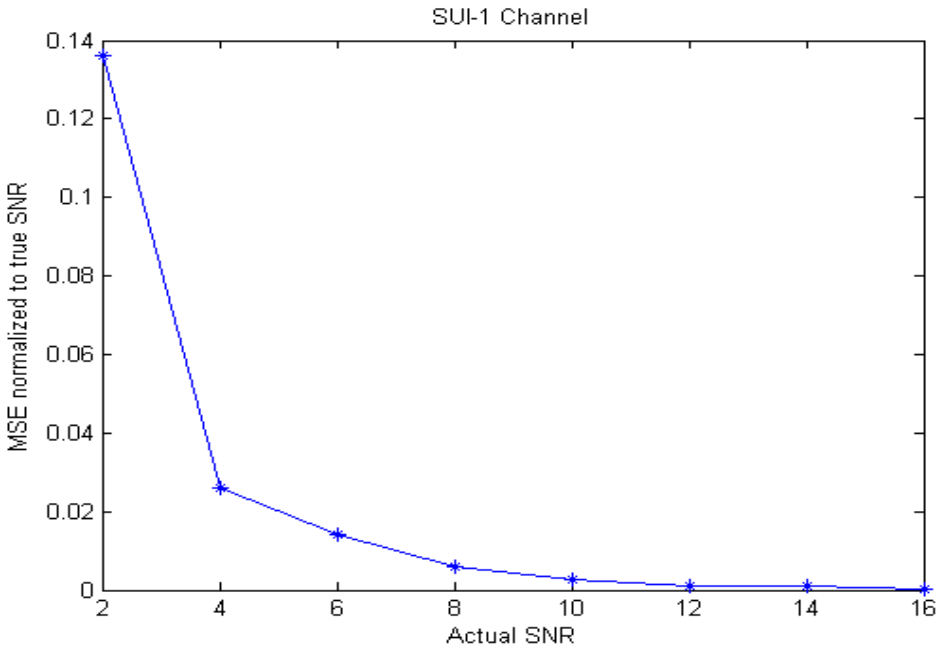


**Fig.4.18 SNR NMSE vs. actual SNR with SUI-1 Channel**

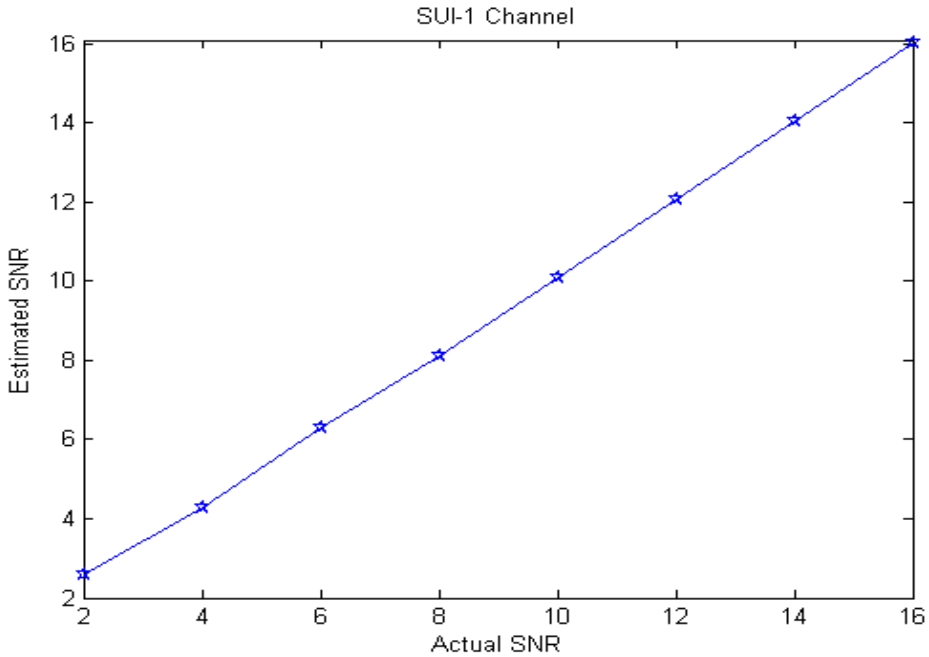


**Fig.4.19 Estimated SNR vs. Actual SNR with SUI-1 Channel**

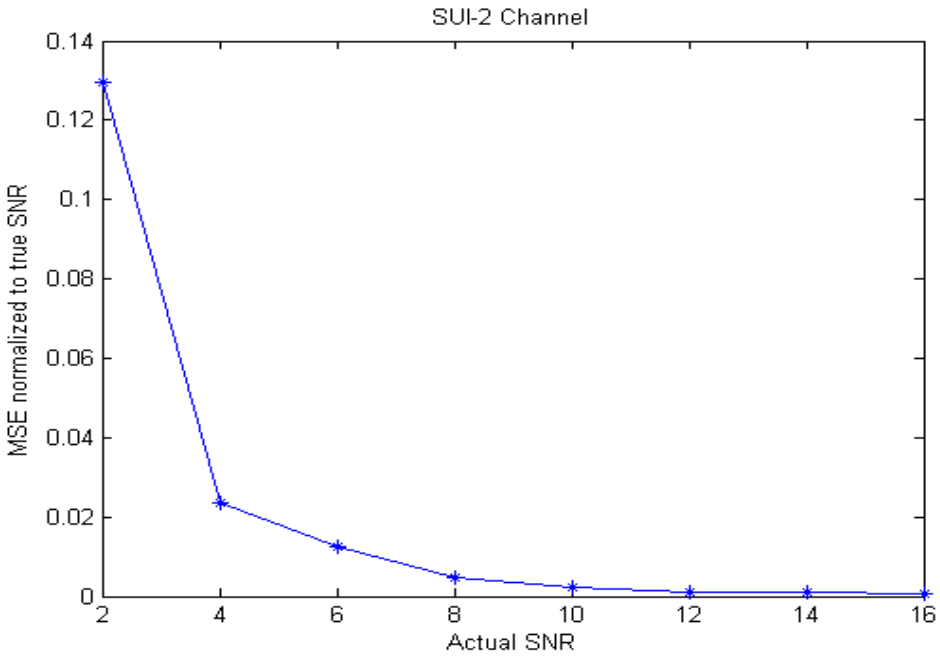


**Fig.4.20 SNR NMSE vs. actual SNR with SUI-2 Channel**

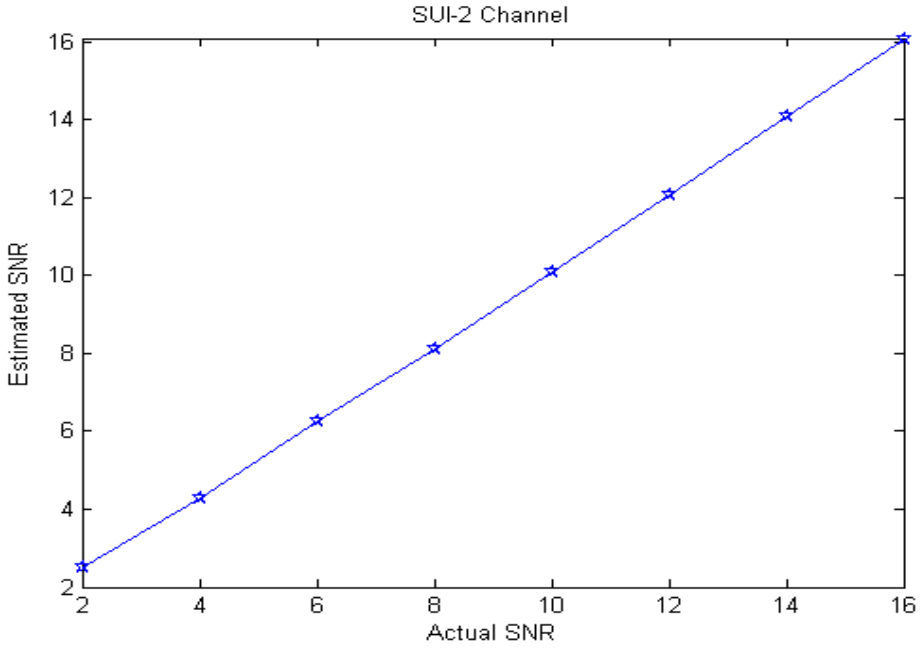


**Fig.4.21 Estimated SNR vs. Actual SNR with SUI-2 Channel**

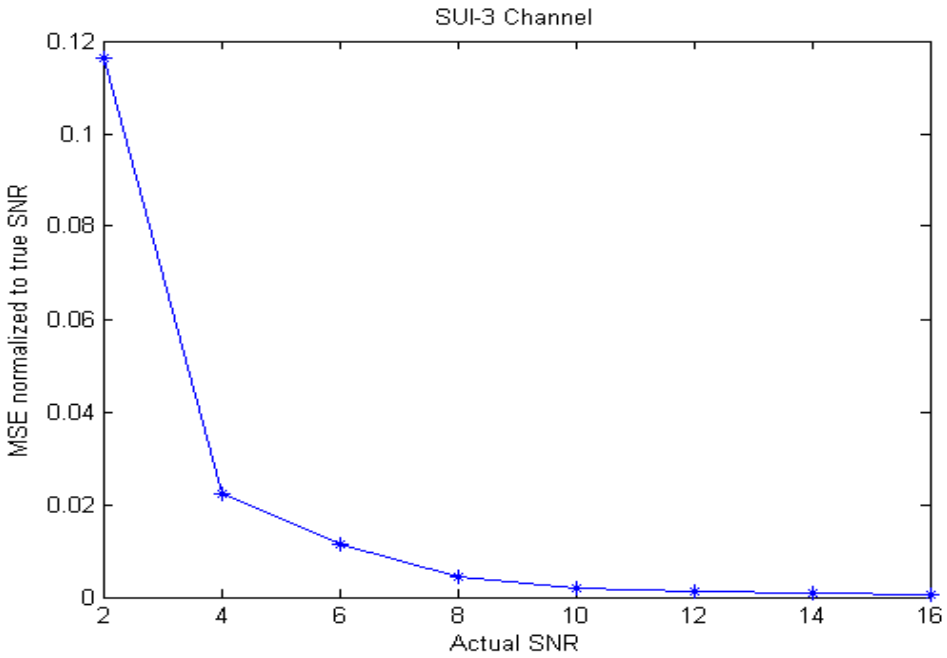


**Fig.4.22 SNR NMSE vs. actual SNR with SUI-3 Channel**

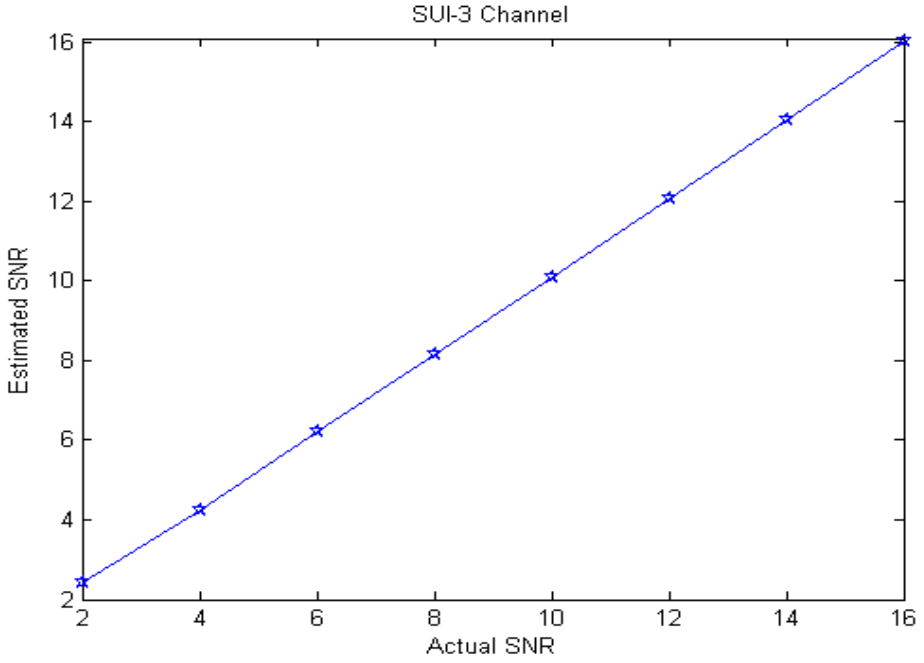


**Fig.4.23 Estimated SNR vs. Actual SNR with SUI-3 Channel**

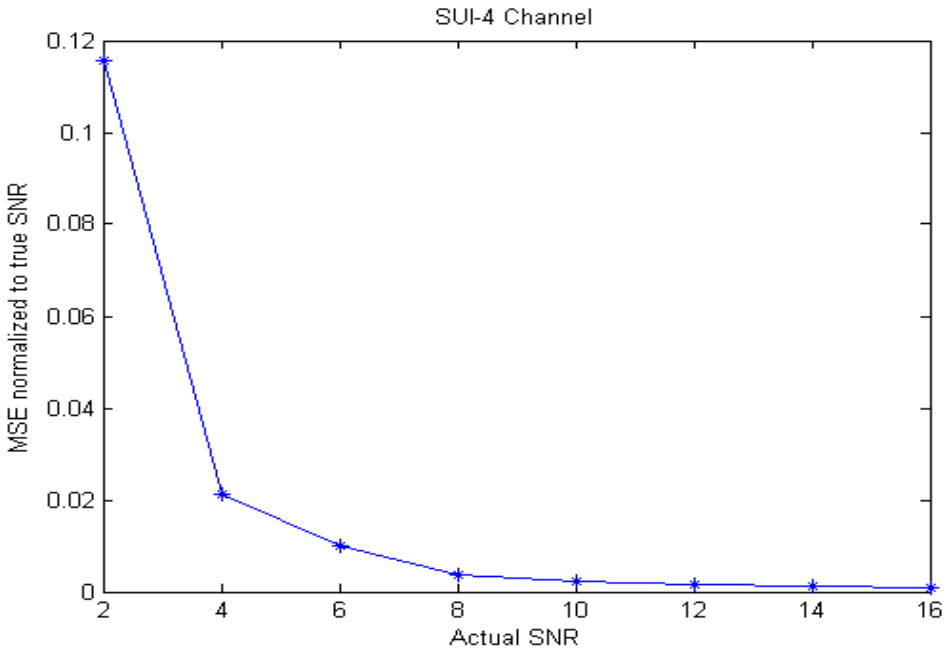


**Fig.4.24 SNR NMSE vs. actual SNR with SUI-4 Channel**

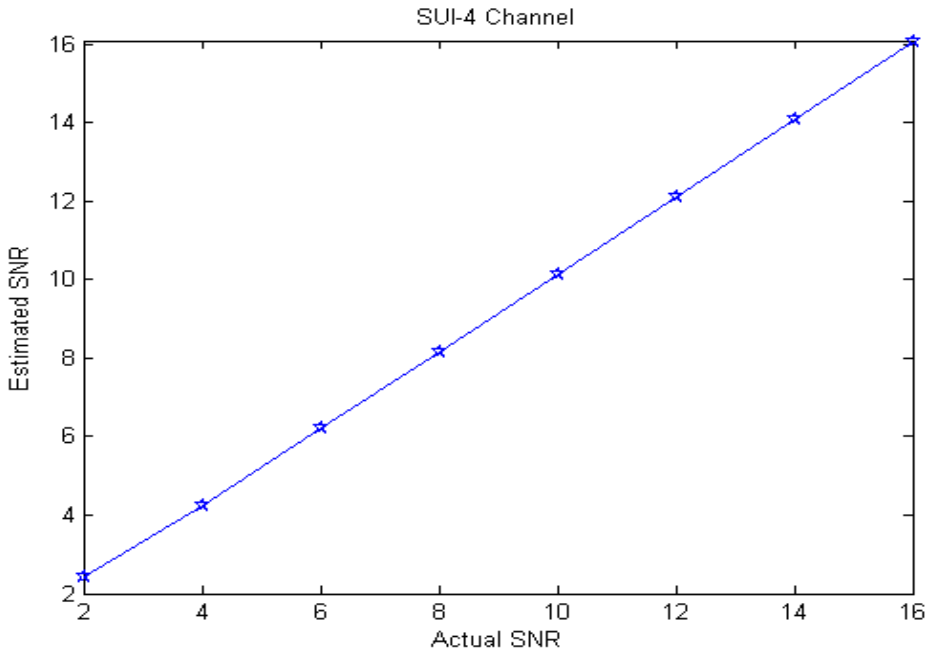


**Fig.4.25 Estimated SNR vs. Actual SNR with SUI-4 Channel**

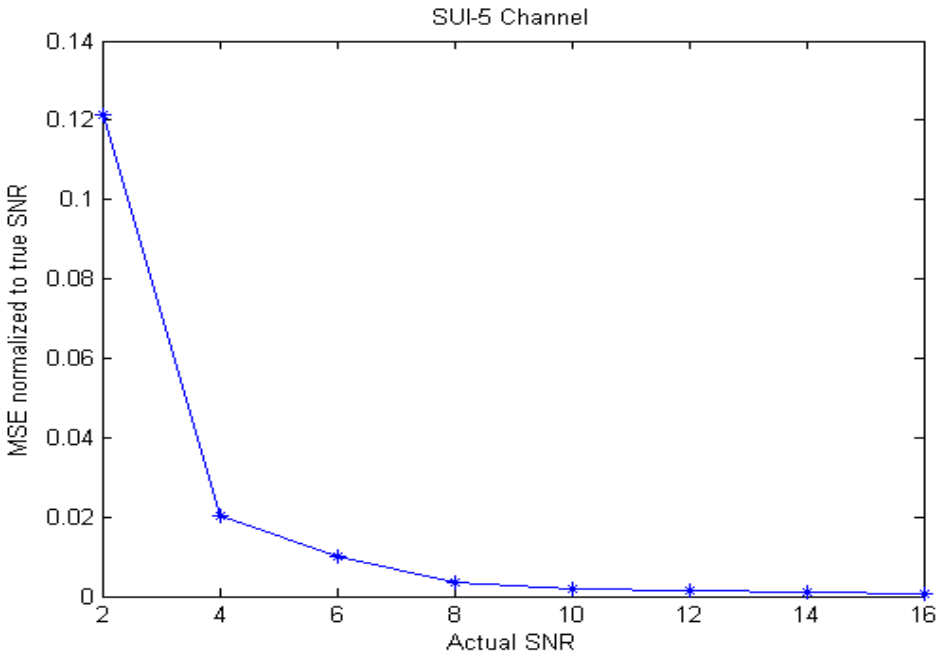


**Fig.4.26 SNR NMSE vs. actual SNR with SUI-5 Channel**

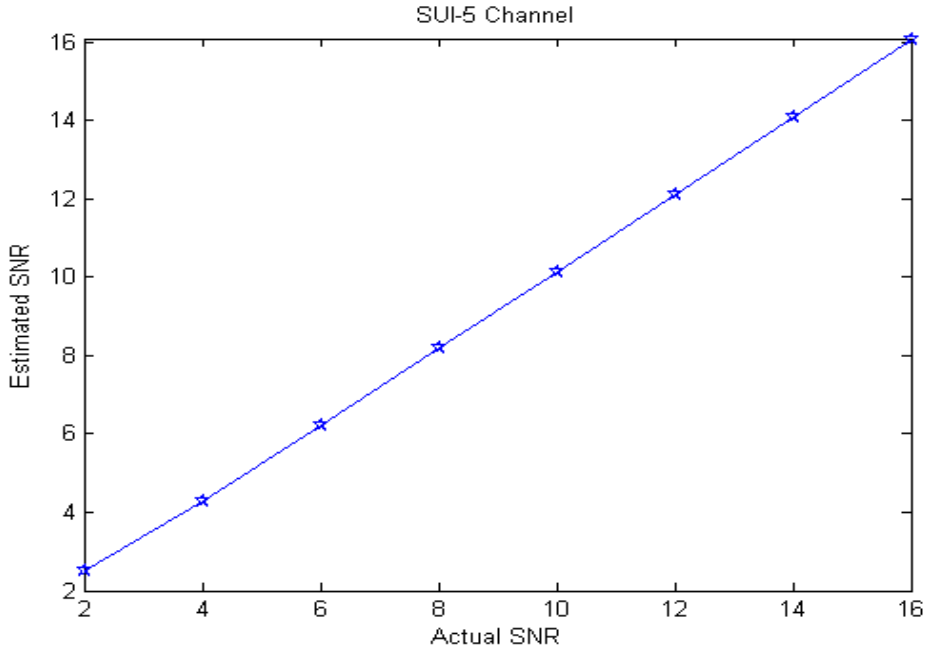


**Fig.4.27 Estimated SNR vs. Actual SNR with SUI-5 Channel**

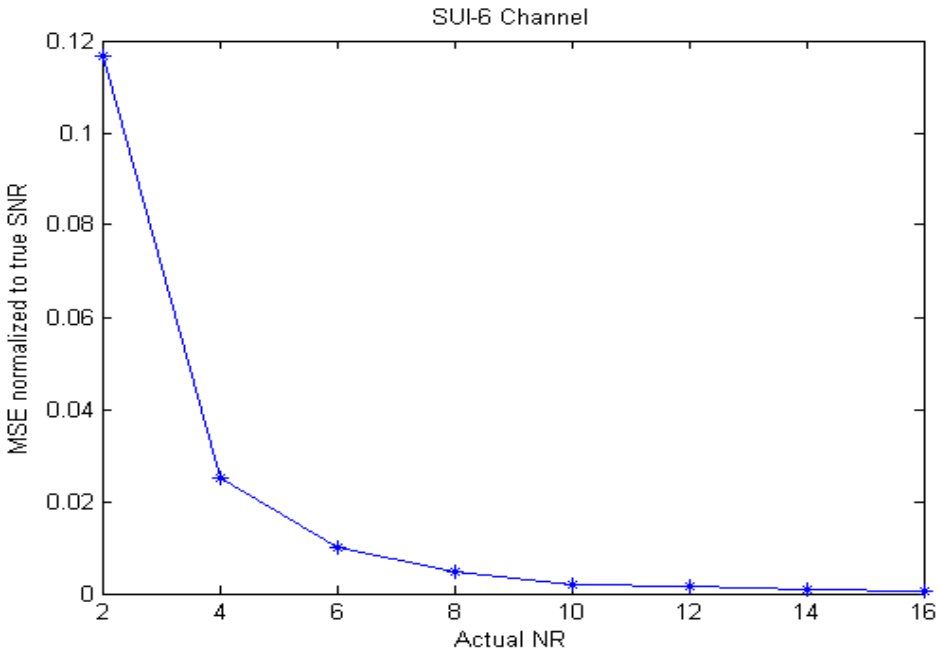


**Fig.4.28 SNR NMSE vs. actual SNR with SUI-6 Channel**

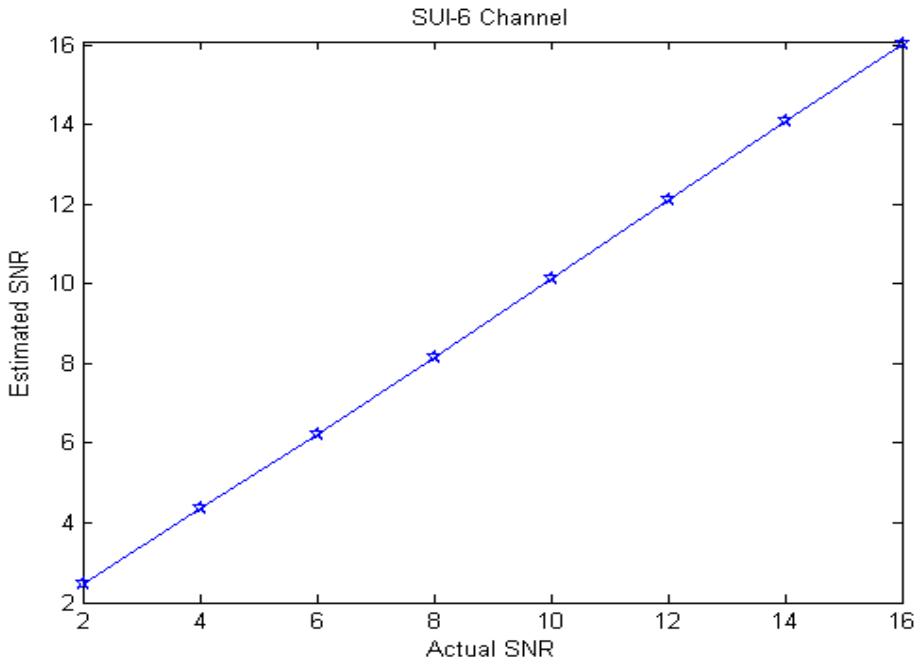


**Fig.4.29 Estimated SNR vs. Actual SNR with SUI-6 Channel**

### 4.2.1.4 Performance over Indoor Channel Model for Wi-Fi

In Fig 4.30 is shown the SNR NMSE is plotted against actual SNR using indoor channel models with 10 taps. Description of indoor channel models is shown in Table 4.4.

It can be seen from the Fig.4.30, that the proposed technique has very small NMSE error. It is observed that the rise in NMSE at small SNR is due to window effect of the system.

In Fig 4.31 estimated SNR is plotted against actual SNR. It can be seen that the estimates of SNR have very small bias and are very close to the actual SNR.

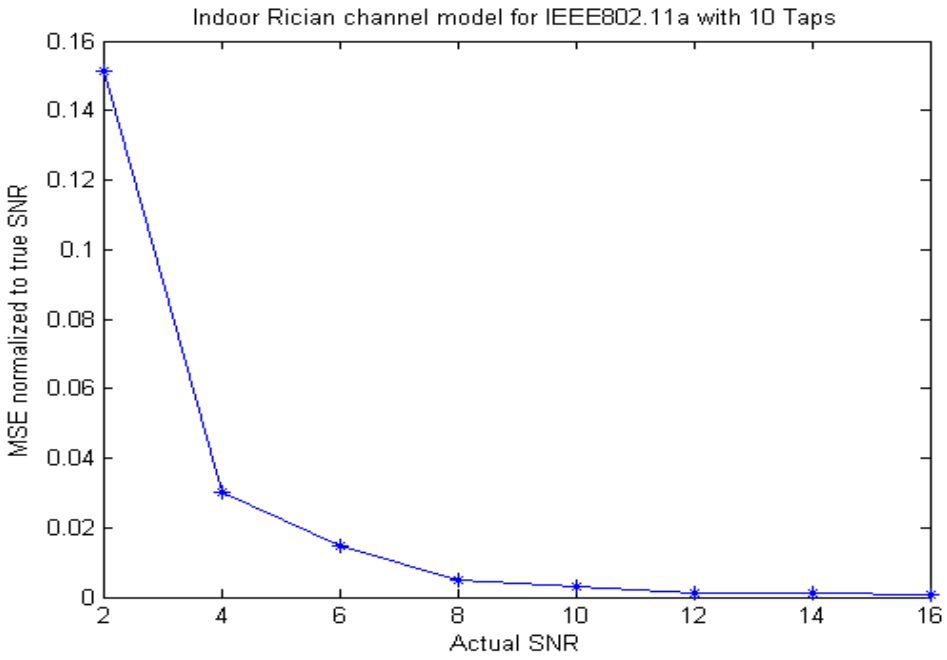


**Fig. 4.30 SNR-NMSE vs. Actual SNR for IEEE802.11a**

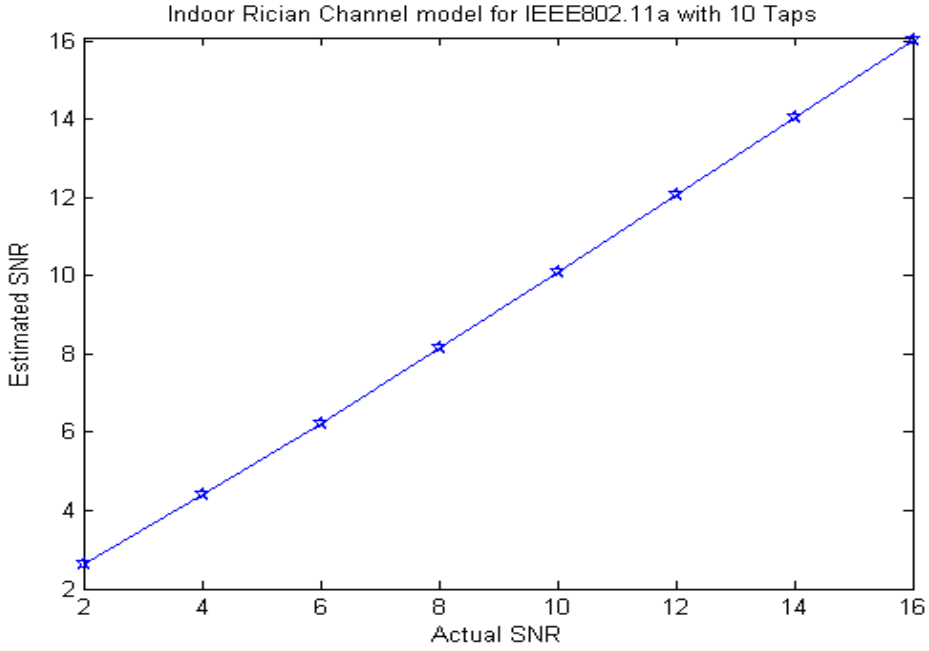


**Fig.4.31 Estimated SNR vs. Actual SNR for IEEE802.11a**

### 4.2.2 Computational Complexity

The proposed estimator has relatively low computational complexity because this is unlike other techniques is able to estimate the SNR from only one OFDM preamble signal. Incidentally the preamble used for the proposed technique is of OFDM systems. As we know, in systems which already employ training sequences for equalization or synchronization, there is no additional throughput penalty and those same known sequences could be used to maximize the performance of a DA-SNR estimator.

The proposed technique stipulates autocorrelation to estimate SNR. Autocorrelation on the received preamble at front end of the receiver and gives rise to two peaks because of two identical halves property of preamble. The signal power is obtained first and noise power later by subtracting the signal power from the magnitude of zero-lag peak. As discussed in detail in chapter 3 that at zero-lag, autocorrelation contains the signal power estimate as well as noise power estimate indistinguishable from each other.

Computational load comes primarily from computing autocorrelation. For an $N$ point long preamble, the autocorrelation ( $\sum_n x_n.x(n+m)$ ) requires $2N^3$ multiplications and $2N^2$ additions.

Subspace estimator has relatively large complexity as compared to proposed estimator. First and foremost, it performs SNR estimation after 30 OFDM symbols beside FFT unlike proposed technique. FFT is the heart of OFDM systems and very complex due to large amount of multiplications. Subspace estimator gives better SNR estimates only after 20 OFDM symbols. It is based on an eigenvector decomposition of the estimated channel correlation matrix. To track the time variation of the SNR, it forms a moving average of the correlation matrix from the $K$ most recent observation matrix, where $K$ is the observed subspace which contains both the channel power and noise power. Minimum descriptive length (MDL) criteria is used to find the number of multipath ($L$) which contains signal subspace and the noise subspace. It is observed that subspace method is

quite complex as it makes use of many calculations and many OFDM symbols to give accurate SNR estimates. To perform comparison of this technique with our proposed technique, we used 30 OFDM symbol for subspace method vs. One OFDM preamble for proposed estimator. The comparison results shown that the proposed technique performs better SNR estimation than subspace estimator.

Reddy estimator has also relatively large computational complexity as compared to proposed estimator. Like subspace method it also perform SNR estimation after FFT. It also gives better SNR estimated with more than 30 OFDM symbols. Averaging window is used to perform averaging across several OFDM symbols as well as across OFDM subcarriers. Due to averaging over large number of OFDM symbols it becomes complex as compared to proposed estimator which makes use of only one OFDM symbol to perform SNR estimation.

Complexity of the SNR estimators discussed above is summarized in the Table 4.5 below. It can be seen that the proposed SNR estimator is computationally less complex to perform SNR estimation. The proposed technique needs only one OFDM preamble to find good SNR estimates as compared to Reddy and subspace which uses 30 OFDM symbols to get good SNR estimates. Reddy and subspace estimators has big complexity because of averaging over so many OFDM symbols and also it makes use of many long and complex calculations to reach a better SNR estimate. Unlike Reddy and subspace estimators, the proposed estimator needs no channel frequency response to find noise power and signal power.

**Table 4.5 Complexity comparison of SNR estimators**

| | |
|---|---|
| **(a) Reddy SNR estimator (Pilot Based), Back-End Estimator** | |
| FFT= $Y_m(k) = DFT\{y_m(n)\} = \sum_n y_m(n) e^{-j2\pi nk/N}$ | complexity ~ $N^3$ |
| Channel Frequency Response = $\hat{H}_m(k) = \frac{Y_m(k)}{S_m(k)}$ | complexity ~ $N^2$ |
| Instantaneous Noise Power ($N$) = $\sigma^2_{N(m)}(k) = \left\| Y_{m(k)} - \hat{X}_{m(k)} \hat{H}_{m(k)} \right\|^2$ | complexity ~ $2N$ |
| Instantaneous Signal power = $\hat{P}_{(s,j)} = \frac{1}{k} \sum_{l=1}^{k} \left\| Y_m(l) \right\|^2$ | complexity ~ $N$ |
| Total complexity of Reddy's Estimator (where 30 shows the number of OFDM symbols used to get better SNR estimates after averaging over these OFDM symbols in both time and frequency domain) | complexity ~ $30\,N^3$ |
| **(b) Subspace SNR Estimator (Pilot Based) , Back-End Estimator** | |
| FFT= $Y_m(k) = DFT\{y_m(n)\} = \sum_n y_m(n) e^{-j2\pi nk/N}$ | complexity ~ $N^3$ |
| Channel Frequency Response = $H_{i,n} = \sum_{l=1}^{L} h_i(i, T_s) e^{-j2\pi \frac{n\tau_l}{NT}}$ | complexity ~ $N$ |
| $\psi = W_p E(h_l \cdot h_l^H) W_p^H$ | complexity ~ $N^2$ |
| Compute Moving Average Estimates of Correlation matrix $\hat{R}(m) = \frac{1}{k} \sum_{i=m-K+1}^{m} H_{i,p} . H_{i,p}^H$ | complexity ~ $N^3$ |
| Estimate the Current Dimensions of the subspace using MDL criteria which gives the number of estimated multipath 'L | |

| | |
|---|---|
| $MDL(k) = -K(M-k)\log\left(\frac{\prod_{i=k+1}^{M} \hat{\lambda} i^{1/(M-k)}}{\frac{1}{M-K}\sum_{i=k+1}^{M} \hat{\lambda}_i}\right) + \frac{1}{2}k(2M-k)\log(K)$ | complexity ~ $N^4$ |
| $\hat{L} = \arg \min_k MDL(k) \qquad k \in \{0,1,2.....,M-1\}$ | complexity ~ $N$ |
| Channel Power= $\hat{\sigma}_s^2 = \frac{1}{M}\left(\sum_{i=1}^{\hat{L}} \hat{\lambda}_i - \hat{L}.\hat{\sigma}_N^2\right)$ | complexity ~ $N$ |
| Noise Power = $\hat{\sigma}_N^2 = \frac{1}{M-\hat{L}}\sum_{i=\hat{L}+1}^{M} \hat{\lambda}_i$ | complexity ~ $N$ |
| Total complexity of subspace estimator (where 30 shows the number of OFDM symbols used to get better SNR estimates after averaging over these OFDM symbols in both time and frequency domain) | complexity ~ $30N^4$ |
| **(c) Proposed SNR Estimator (Preamble Based), Front-End Estimator** | |
| Autocorrelation of received signal = $R_{yy}(m) = R_{xx}(m) + R_{nn}(m)$ | complexity ~ $2N^3$ |
| Total complexity of developed estimator = | complexity ~$2N^3$ |

## 4.2.3 Sensitivity Analysis

To analyze the sensitivity of developed estimator, we derive the estimated SNR with respect to correlation peaks at (*L-N/2*, *L-N* and *L*) that used to estimate the SNR.

As we know, SNR estimated is

$$\hat{SNR} = \frac{\hat{P}_o}{\hat{\sigma}_N^2} = \frac{2R_{yy}(L - N/2) - R_{yy}(L-N)}{R_{yy}(L) - 2R_{yy}(L - N/2) - R_{yy}(L-N)} \tag{4.2}$$

To perform sensitivity analysis let us suppose that

$$\hat{SNR} = \frac{2x_1 - x_2}{x_3 - (2x_1 - x_2)} \tag{4.3}$$

where,

$x_1 = R_{yy}(L - N/2)$

$x_2 = R_{yy}(L - N)$

$x_3 = R_{yy}(L)$

Any change in the estimated ($\hat{SNR}$) SNR is given by

$$\Delta\hat{SNR} = \frac{\partial\hat{SNR}}{\partial x_1}.\Delta x_1 + \frac{\partial\hat{SNR}}{\partial x_2}.\Delta x_2 + \frac{\partial\hat{SNR}}{\partial x_3}.\Delta x_3 \tag{4.4}$$

where

$$\begin{aligned}
\frac{\partial\hat{SNR}}{\partial x_1} &= \frac{2 - x_2/x_3}{x_3 - 2 + x_2/x_1} \\
\frac{\partial\hat{SNR}}{\partial x_1} &= \frac{2x_1/x_2 - 1}{x_3/x_x - 2x_1/x_2 + 1} \\
\frac{\partial\hat{SNR}}{\partial x_1} &= \frac{2x_1/x_3 - x_2/x_3}{1 - 2x_1/x_3 + x_2/x_3}
\end{aligned} \tag{4.5}$$

The parameter of eq. 4.5 describe the sensitivity of estimated SNR as a function of x1, x2 and x3. The sensitivity of estimated SNR with respect to (*L-N*) peak, (*L-N/2*) peak and (*L*) peak is plotted against actual SNR value in Fig 4.32, Fig 4.33 and Fig 4.34. The SNR is varied from 1 dB to 16 dB.

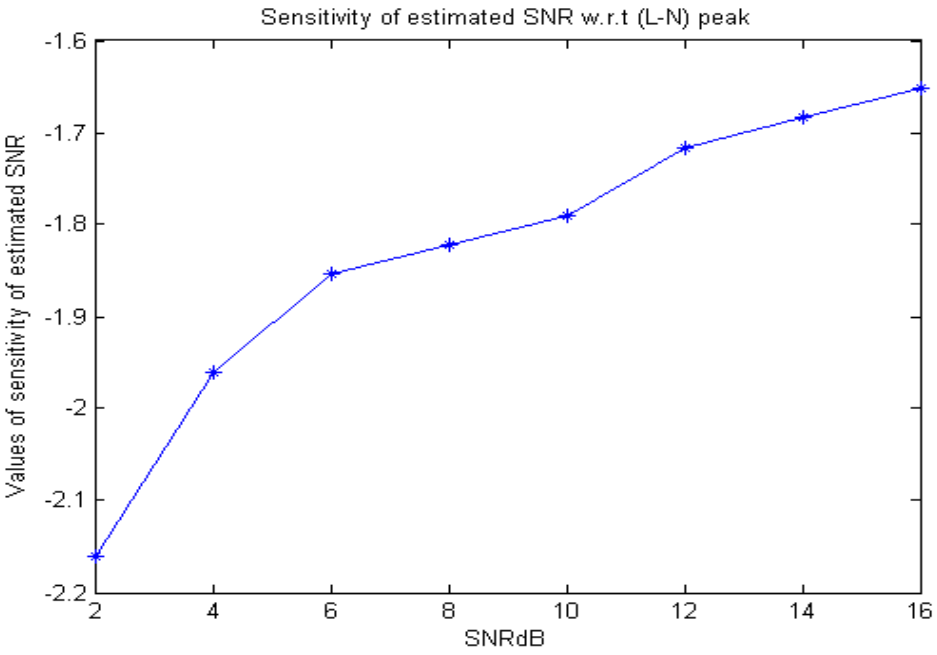


**Fig.4.32 : Sensitivity of estimated SNR w.r.t. (L-N) peak**

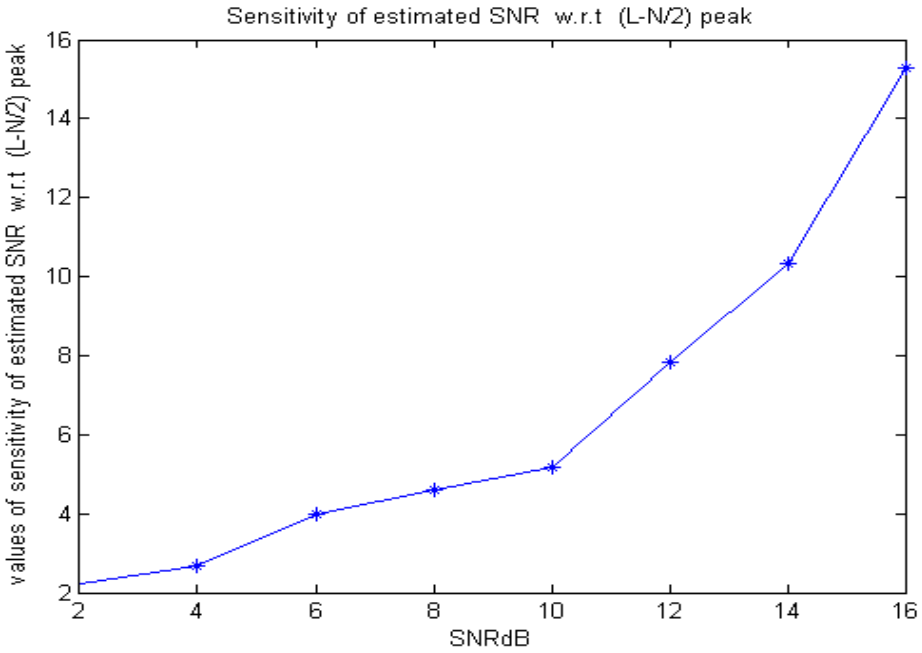


**Fig.4.33 : Sensitivity of estimated SNR w.r.t. (L-N/2) peak**

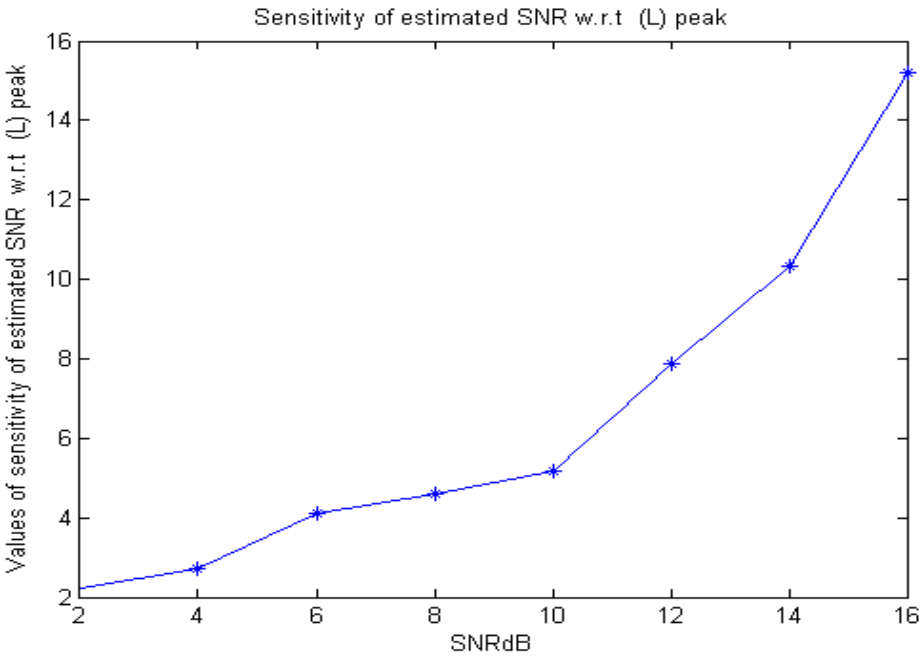


**Fig.4.34 : Sensitivity of estimated SNR w.r.t. (L) peak**

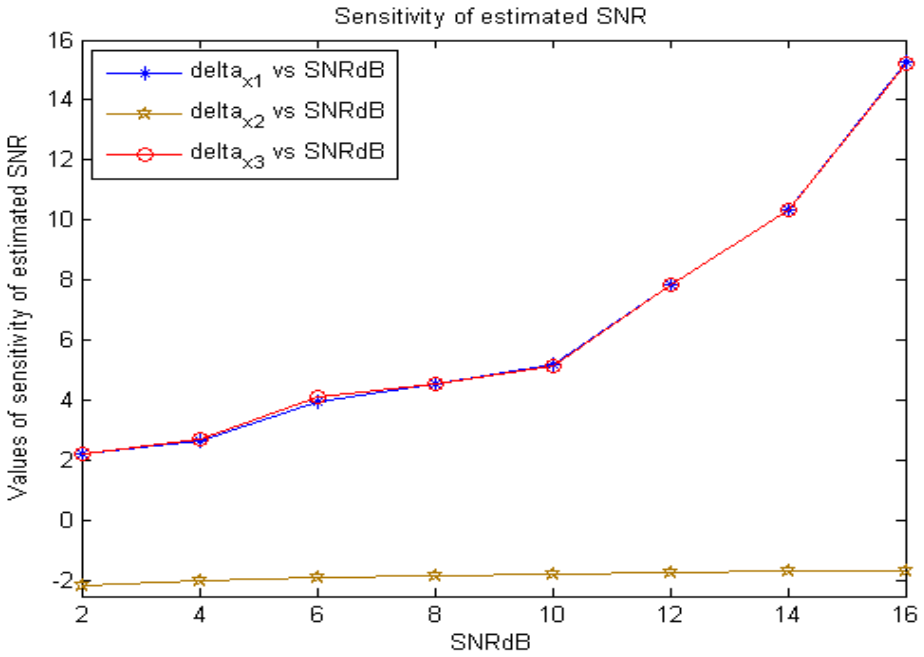


**Fig.4.35 : Combined results of sensitivity of estimated SNR**

It is observed from the Fig. 4.32, Fig 4.33 and Fig. 4.34, that the estimated SNR is more sensitive to (*L*-*N*) peak and (*L*) peak.

In summary, the three criteria used for the search of good SNR estimator are:

- Accuracy of SNR estimates
- Minimum computational complexity
- Easy to implement.

The results show that the proposed estimator fulfill the criteria of good SNR estimator

## 4.3 Analysis Results of SNR Estimation Technique for Multipath Channel with Colored Noise using Wavelet-Packet Transform in OFDM Systems

The technique describe in section 4.2 is extended to obtaining noise power estimates of colored noise using wavelet-packet based filter bank analysis of the noise. The proposed technique is compared with Reddy's estimator for colored noise in OFDM system with parameters given in Table 3.4 as shown in chapter 3. SNR is varied from 1 dB to 20 dB for each sub-band and the mean-squared error (MSE) is derived for the estimated SNR from 2000 trials according to the following formula

$$MSE = \frac{1}{2000} \sum_{i=1}^{2000} \{\hat{SNR}(i) - SNR\}^2 \tag{4.6}$$

Figure 4.36 shows the mean-square-error performance of the proposed and conventional algorithms in colored noise. The mean-squared-error between the actual SNR and estimated SNR values in each sub-band are calculated and averaged. As can be seen the proposed algorithm performs much better than Reddy's SNR estimation.

Fig.4.37 shows the plot of actual SNR vs. estimated SNR over all OFDM signal. SNR is estimated in each sub-band first than averaging over all sub-band is performed to get a global (over all sub-carriers) SNR estimates.

Therefore, the proposed approach estimates both local (within smaller sets of subcarriers) and global (over all sub-carriers) SNR values. The short term local estimates calculate the noise power variation across OFDM sub-carriers. These estimates are specifically very useful for adaptive modulation, and optimal soft value calculation for improving channel decoder performance.

The results show that the proposed estimator gives better performance in SNR estimation as compared to Reddy estimator.

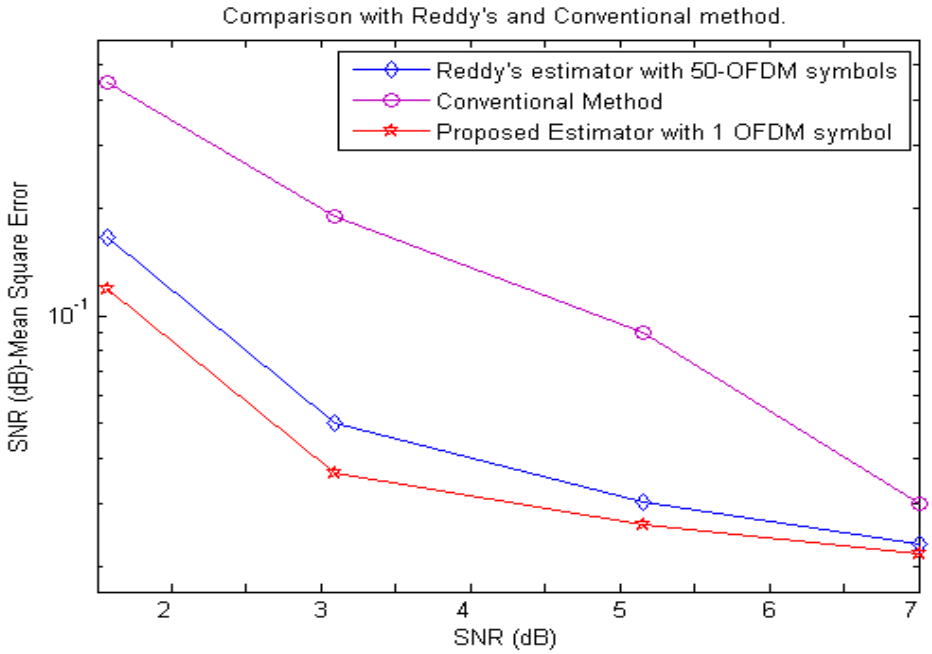


**Fig.4.36. Mean-square-error performance of the proposed technique with colored noise**

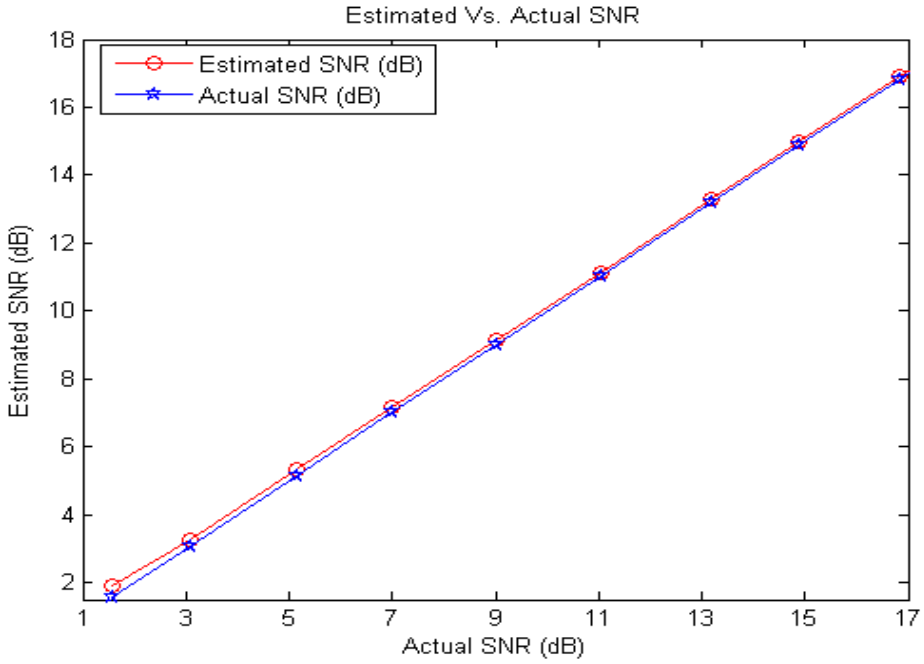


**Fig.4.37. Estimated SNR vs. Actual SNR with colored noise**

### 4.3.1 Performance Comparisons of colored noise estimator

Fig.4.36 shows that the proposed technique gives very accurate estimates of colored noise variation which is very useful for adaptive modulation. Proposed technique is compared with Reddy estimator for colored noise. From the results it can be shown that the proposed technique, with only one OFDM symbol, perform better than Reddy estimator which is using 50 OFDM symbols. The mean squared error of proposed technique is much lower than Reddy estimator.

Fig.4.37 shows that the SNR estimates of colored noise using proposed technique is very close to the actual SNR values and has very small bias.

## 4.4 Summary

In this chapter, the results of proposed front-end noise power and SNR estimation technique for white noise as well as for colored noise are discussed. The simulations are conducted in both frequency non-dispersive and dispersive channels with real additive white Gaussian noise (AWGN) and also colored noise. The results of SNR estimation technique for AWGN in OFDM systems are presented and compared with previously techniques in terms of normalized mean squared error (NMSE) and estimated SNR. The results of SNR estimation technique for colored noise using wavelet-packet in OFDM systems are shown and compared with previous techniques in terms of mean squared error (MSE) and estimated SNR. The results show that the proposed technique gives better performance than previously published SNR estimators. It is observed that the proposed technique can estimate local statistics of the noise power when the noise is colored. The proposed estimator has relatively low computational complexity because it makes use of only one OFDM preamble signal to find the SNR estimates. The proposed estimator is fulfills the criteria of best SNR estimator because it is unbiased (or exhibits the smallest Bias) and has the smallest variance of SNR estimates as shown from results clearly.